



## Excellent adhered thick diamond-like carbon coatings by optimizing hetero-interfaces with sequential highly energetic Cr and C ion treatment



Liangliang Liu<sup>a</sup>, Zhongzhen Wu<sup>a, b, \*</sup>, Xiaokai An<sup>a</sup>, Shu Xiao<sup>a</sup>, Suihan Cui<sup>a</sup>, Hai Lin<sup>a</sup>, Ricky K.Y. Fu<sup>b</sup>, Xiubo Tian<sup>a</sup>, Ronghua Wei<sup>c</sup>, Paul K. Chu<sup>b</sup>, Feng Pan<sup>a, \*\*</sup>

<sup>a</sup> School of Advanced Materials, Peking University Shenzhen Graduate School, Shenzhen 518055, China

<sup>b</sup> Department of Physics and Materials Science, City University of Hong Kong, Tat Chee Avenue, Kowloon, Hong Kong, China

<sup>c</sup> Southwest Research Institute, 6220 Culebra Road, San Antonio, USA

### ARTICLE INFO

#### Article history:

Received 14 August 2017

Received in revised form

28 October 2017

Accepted 4 November 2017

Available online 7 November 2017

#### Keywords:

Thick DLC films

Graded interlayer

Energetic ion beam bombardment

Adhesion

### ABSTRACT

Diamond-like carbon (DLC) coatings have attracted much attention due to their excellent hardness, low friction, and superior corrosion resistance. Unfortunately, the poor adhesion caused by internal stress limits the typical thickness to below 3–5  $\mu\text{m}$ . This paper presents a novel interlayer design and interface engineering and the induced excellent adhesion of thick diamond-like carbon (DLC) coatings on a high speed steel substrate. The interlayer has fundamentally a graded Cr/Cr<sub>x</sub>/CrC/DLC structure, but various treatments to the hetero-interfaces have been conducted including sequential energetic ion bombardments with Cr at the substrate/Cr interface using high-power impulse magnetron sputtering (HiPIMS) and with C at the CrC/DLC interface using an anode layer ion source. It has been observed that the critical load has been improved from 18 N for a single Cr interlayer to 77 N for a Cr/Cr<sub>x</sub>/CrC interlayer for thick DLC coatings of 13  $\mu\text{m}$ . Using the same design, a very high critical load of 73 N has been achieved on the ultra-thick DLC coating of 50  $\mu\text{m}$ . This interlayer design has allowed the deposition of a DLC coating that is not only thick but also hard with excellent tribological properties. The DLC coatings have a high hardness of >18 GPa, a low friction coefficient of 0.12 and a low wear rate of  $(1.7 \pm 0.2) \times 10^{-15} \text{ m}^3/\text{N}\cdot\text{m}$ . This paper discusses the effect of the ion bombardment of the interlayer on the coating adhesion and the strengthening mechanisms.

© 2017 Elsevier B.V. All rights reserved.

### 1. Introduction

Diamond-like carbon (DLC) coatings, which are amorphous coatings consisting of  $\text{sp}^3$  bonding of diamond and  $\text{sp}^2$  bonding of graphite, have demonstrated excellent properties such as high hardness, low friction, and superior corrosion resistance [1–4] and have been used in cutting tools, dies, and petroleum pipelines [5]. However, the high internal stress inherent to thick DLC films results in poor adhesion with many types of substrates. In practice, the thickness of DLC coatings is limited to 3–5  $\mu\text{m}$  [6] which is insufficient for some applications that demand high load, high speed,

and long service life such as in the aerospace and automotive industries.

Two strategies have been proposed to increase the thickness of DLC coatings. First, the internal stress can be reduced by doping with Si, W, Al [1,7–9], and other elements. However, in spite of improved film adhesion, the hardness, friction, and corrosion resistance are often compromised [9–11]. Second, an interlayer can reduce the physical mismatch between DLC coatings and substrates to improve adhesion [12,13]. However, the interface between the interlayer and substrate and that between the interlayer and coating are still mismatched and they become the primary weak links for failure. In our previous work [14], ion implantation was used to improve the interface between a stainless steel substrate and the top coating of CrN. To obtain the micro-particles free and highly ionized Cr ion beams, high-power impulse magnetron sputtering (HiPIMS) was used for the ion implantation. The energy of highly ionized metal plasmas obtained by HiPIMS was controlled

\* Corresponding author. School of Advanced Materials, Peking University Shenzhen Graduate School, Shenzhen 518055, China.

\*\* Corresponding author.

E-mail addresses: [wuzz@pkusz.edu.cn](mailto:wuzz@pkusz.edu.cn) (Z. Wu), [Panfeng@pkusz.edu.cn](mailto:Panfeng@pkusz.edu.cn) (F. Pan).

by the pulsed bias similar to the situation in plasma immersion ion implantation & deposition (PIII&D).

In this study, using the similar strategy, we took one step further to improve the adhesion of thick and ultra-thick DLC coatings (13–50  $\mu\text{m}$ ). Together with the pulsed bias on the substrates, the HiPIMS was used to increase the interlayer strength between the Cr layer and the substrate, while an anode layer ion source was used to strengthen the CrC/DLC interface since the ion source produces dense and highly ionized C plasma. Furthermore, a graded Cr/CrC<sub>x</sub>/CrC interlayer structure was engineered to increase the adhesion strength and reduce the stress. Using the best interlayer design, a high critical load of 77 N and 73 N have been achieved for the 13  $\mu\text{m}$  and 50  $\mu\text{m}$  thick DLC coatings. The effect of the interlayers design on the coating adhesion and the strengthening mechanisms will be discussed.

## 2. Experimental details

Silicon (100) and High-speed steel (HSS) substrates were used in this study. The HSS samples ( $\phi 25 \times 4$  mm) were polished with abrasive SiC papers from 320 to 1500 grits and finally with 1  $\mu\text{m}$  diamond paste on velvet cloth. All samples were ultrasonically cleaned sequentially in alcohol, acetone, and deionized water for 30 min each and then dried with hot air blow before they were installed into the processing chamber. The DLC depositions were carried out in a multifunctional plasma surface modification and deposition system (100 cm in dia. by 80 cm high) shown in Fig. 1. After the vacuum system was evacuated to a base pressure of  $8 \times 10^{-4}$  Pa, Ar glow discharge plasma was generated and the substrates were sputter-cleaned for 20 min (Ar flowrate of 40 sccm, chamber pressure of 0.8 Pa and sample bias of  $-600$  V). Then an interlayer was deposited. Four different interlayer structures (Cr, Cr/CrC, Cr/CrC<sub>x</sub> and Cr/CrC<sub>x</sub>/CrC) were designed to investigate the DLC coating adhesion strength. The processing parameters for the interlayers are listed in Table 1. In Stage I, for all experiments a Cr layer was ion implanted/deposited with Cr from a target (99.9 at%) by HiPIMS with the pulsed voltage, frequency and pulse width of 750 V, 50 Hz and 300  $\mu\text{s}$ , respectively, in Ar (30 sccm, 99.999% purity). In order to avoid instable discharge of HiPIMS, middle frequency (MF) of a total power of 900 W (450 V, 2 A) was imposed. The bias voltage on the samples was  $-800$  V to improve the Cr/HSS interface adhesion. The processing time was 2 min.

**Table 1**

Important instrumental parameters in the different stages of interlayer fabrication.

Samples	Stage I (Cr)		Stage II (CrC <sub>x</sub> )		Stage III (CrC)			
	Bias (V)	Time (min)	C <sub>2</sub> H <sub>2</sub> (sccm)	Bias (V)	Time (min)	C <sub>2</sub> H <sub>2</sub> (sccm)	Bias (V)	Time (min)
Cr/DLC	-800	2	0	-100	8	–	–	–
Cr/CrC/DLC	-800	2	–	–	–	30	-100	8
Cr/CrC <sub>x</sub> /DLC	-800	2	0–30	-100	8	–	–	–
Cr/CrC <sub>x</sub> /CrC/DLC	-800	2	0–30	-100	8	30	-100	2

In Stage II, for the first coating (Cr/DLC), while the HiPIMS deposition parameters for Cr were maintained, the bias voltage was reduced to  $-100$  V. The processing time was 8 min to form a thicker Cr layer. For the third (Cr/CrC<sub>x</sub>) and the fourth (Cr/CrC<sub>x</sub>/CrC) coatings, while the Cr deposition was still in progress (with the reduced bias voltage of  $-100$  V), C<sub>2</sub>H<sub>2</sub> (99.8% purity) was gradually bled into the vacuum system at a flowrate from 0 sccm to 30 sccm to form CrC<sub>x</sub>. The processing time was also 8 min. For the second coating, after the 2 min Cr deposition at the high voltage bias ( $-800$  V), without the ramping, 30 sccm of C<sub>2</sub>H<sub>2</sub> was directly fed into the vacuum system to form the CrC coating as indicated in Stage III and this process also took 8 min. For the fourth coatings, after the Stage II CrC<sub>x</sub> coating when C<sub>2</sub>H<sub>2</sub> reached the full flowrate of 30 sccm, the process was extended for 2 more minutes.

Finally, the DLC coating was deposited using an anode layer ion source for 10 h at a power of 300 W at a pressure of 0.5 Pa in a gas mixture of 10 sccm Ar and 45 sccm C<sub>2</sub>H<sub>2</sub> for all four tests and the sample holder was fixed without rotating. To enhance the interface between the DLC film and interlayer, a negative pulsed voltage (7.5 kV, 50 Hz, 100  $\mu\text{s}$ ) was applied.

The thickness and morphology were measured by field-emission scanning electron microscopy (FE-SEM, ZEISS SUPRA<sup>®</sup> 55) equipped with energy-dispersive X-ray spectrometer (EDS) and the detailed interfacial structure was examined by transmission electron microscopy (TEM, JEM-3200FS). The bonding structure was determined at room temperature by high-resolution confocal Raman scattering (Horiba LAabRam HR VIS) with a 532 nm laser as the excitation source and X-ray photoelectron spectroscopy (ESCALAB 250X, Thermo Fisher, England). The microhardness was determined by nanoindentation (Hysitron TI 950) in the Nano Dynamic Mechanical Analysis mode. A scratch test instrument

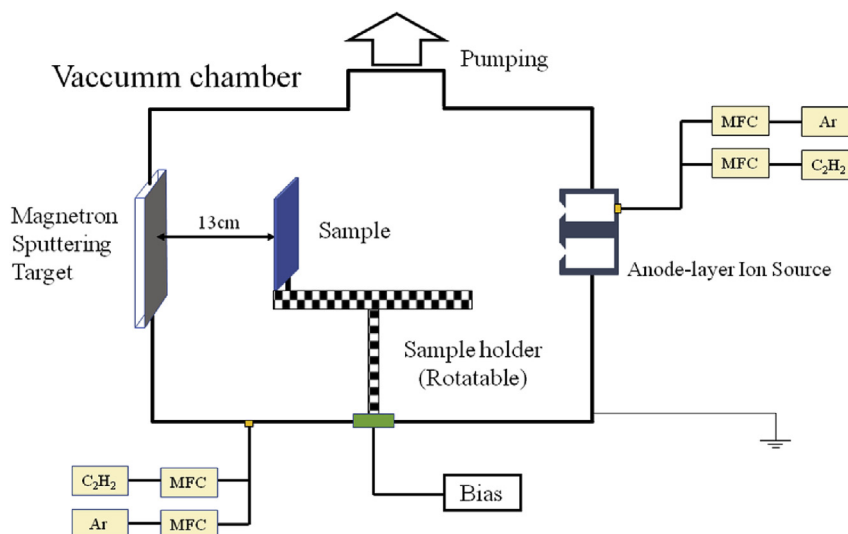


**Fig. 1.** Schematic of the deposition system and positioning of the substrate in relation to the plasma sources.

(WS-2005, Zhongke Kaihua Technology, China) equipped with acoustic emission was employed to study the adhesion strength between the film and substrate. The load was progressively increased from 0 N to 100 N at 3 mm/min and 50 N/min. A ball-on-disk tester (Rtec MFT-5000) was used to determine the friction coefficients and wear resistance at a relative humidity of  $65 \pm 1\%$  RH and temperature of  $25 \pm 1$  °C. A  $\Phi 3$  mm  $\text{Si}_3\text{N}_4$  ball was used against the coatings at 4 N and 200 rpm with a wear radius of 5 mm.

### 3. Results

Fig. 2 shows the cross-sectional images of the DLC coatings and different interlayer structures deposited on Si (100). The interlayer and DLC coatings can be observed and the total thickness of the coatings is about 13  $\mu\text{m}$  including the interlayer with a thickness of 0.8–1.0  $\mu\text{m}$ . The DLC layers have a dense amorphous structure with no apparent defects. The interlayer morphology is different depending on the deposition conditions. Only a Cr interlayer is observed in Fig. 2(a) and the Cr layer shows two different morphologies depending on the thickness. Owing to ion bombardment ( $-800$  V), the 200 nm Cr interlayer close the substrate has a small columnar structure and the cluster size of the column increases when the bias is reduced to  $-100$  V. An obvious interface can be observed in Fig. 2(b) because of the sudden change in the  $\text{C}_2\text{H}_2$  flow and the bottom layer shows much a denser and smaller structure compared to the top layer. The double-layer structures are shown in Fig. 2(c) and (d). The interface between the interlayer and DLC coating is more obvious in Fig. 2(c) than Fig. 2 (d), indicating the effects of the CrC layer with superfluous  $\text{C}_2\text{H}_2$ . Moreover, in order to detect the distribution of C and Cr elements in the interlayers, EDS is performed on the label arrow lines in Fig. 2. Fig. 3 gives the C and Cr distributions on different sample interlayers. The Cr/CrC interlayer in Fig. 3(b) shows a rapid increase of C element in the Cr/CrC interface. The C distributions of Cr/CrCx and Cr/CrCx/CrC in Fig. 3(c) and (d) show a gradually increase depending on the  $\text{C}_2\text{H}_2$  flow.

To determine the microstructure and bonding of the DLC coatings, the Raman scattering spectra are presented in Fig. 4 and Table 2. The typical Raman spectra of DLC consists two

characteristic bands (G and D). The G band represents the stretching mode of  $\text{sp}^2$  carbon atoms in both rings and chains, whereas the D band is related to the breathing mode of  $\text{sp}^2$  in the rings [15]. Thus, the intensity, peak position, and full-width at half-maximum (FWHM) of the D and G bands reflect the quality of the DLC films [16]. As the spectra are quite similar, only one spectrum is shown in Fig. 4 which is deconvoluted into the D peak and G peak using Gaussian fitting. As shown in Table 2, no obvious difference can be observed from the band position and FWHM. The ratios of the D and G band ( $I_D/I_G$ ) are in the range between 0.573 and 0.577 indicative of a large percentage of  $\text{sp}^3$ .

XPS is employed to disclose the surface bonding states. The XPS C1s spectra in Fig. 5 show a large asymmetrical peak due to the different bonding states of carbon atoms [17]. No distinct difference is found from the peak position and FWHM. The C1s peak can be deconvoluted into two peaks assigned to the C–C  $\text{sp}^2$  hybridized carbon atoms (284.3 eV) and C–C  $\text{sp}^3$  hybridized carbon atoms (285.2 eV). The percentage of  $\text{sp}^3$  hybridized carbon atom is estimated from the ratio of the C–C  $\text{sp}^3$  peak area to the total C1s area and they are ( $53.6 \pm 0.2$  %), ( $54.6 \pm 0.2$  %), ( $54.6 \pm 0.2$  %), and ( $54.5 \pm 0.2$  %) for the four different samples.

Nanoindentation is performed to evaluate the mechanical properties (5 points for each sample). The hardness(H) and elastic moduli (E) of the coatings are shown in Fig. 6. The hardness of the four samples are 17.72 GPa, 17.97 GPa, 18.37 GPa and 18.17 GPa, respectively, and no significant difference occurs considering the measure errors. This is quite good for hydrogenated DLC (including DLC with dopants such as F, N, Si, and metals) [1,6]. The elastic modulus is about 120 GPa (118 GPa for Cr/DLC, 119 GPa for Cr/CrC/DLC, 121 GPa for Cr/CrCx/DLC and 120 GPa for Cr/CrCx/CrC/DLC) thereby giving rise to large  $H^3/E^2$  and H/E ratios of 0.41 and 0.15, respectively, as shown in Table 3.

Fig. 7 presents the friction coefficients and wear rates of the DLC coatings determined by ball-on-disk tests with a  $\text{Si}_3\text{N}_4$  counterpart for 2 h. The friction coefficient (Fig. 7(a)) of the HHS substrate starts at 0.15, increases thereafter, and stabilizes at about 0.7 finally. The friction coefficients of the DLC coatings are large in the beginning of the test but decrease to 0.12 quickly until the end, and can indicate

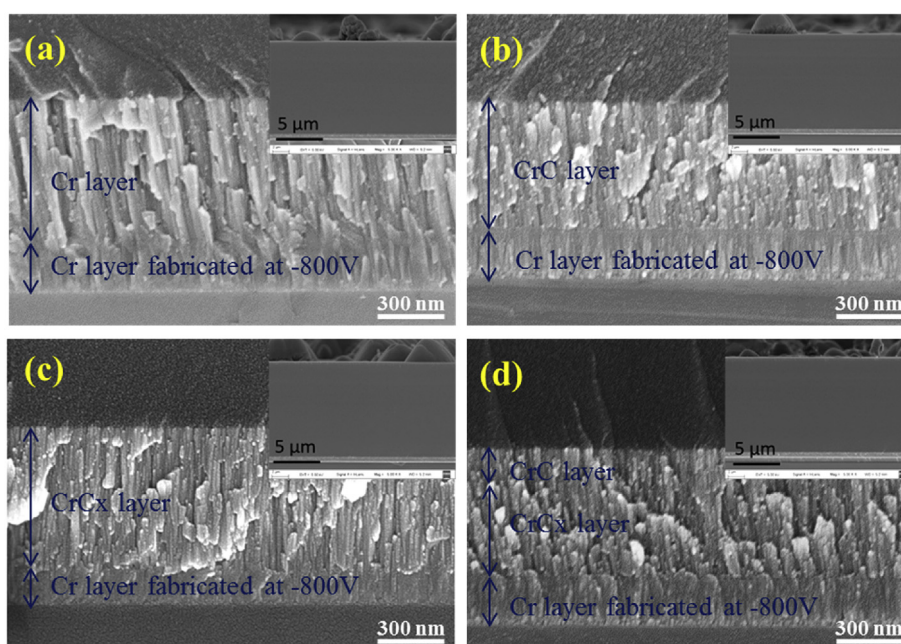


Fig. 2. SEM cross-sectional images: (a) Cr/DLC, (b) Cr/CrC/DLC, (c) Cr/CrCx/DLC, and (d) Cr/CrCx/CrC/DLC.

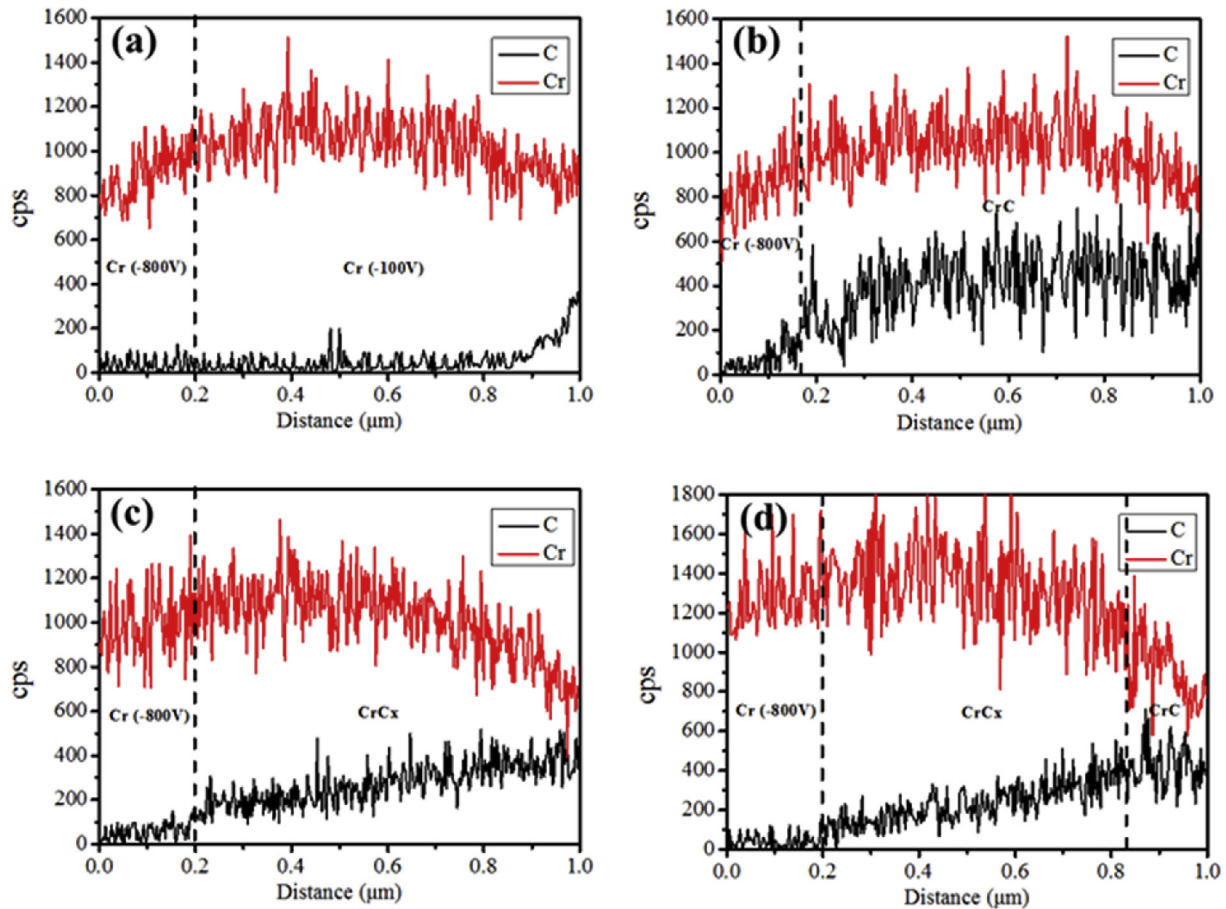


Fig. 3. The C and Cr cross-sectional distribution of different interlayers: (a) Cr, (b) Cr/CrC, (c) Cr/CrC<sub>x</sub>, and (d) Cr/CrC<sub>x</sub>/CrC.

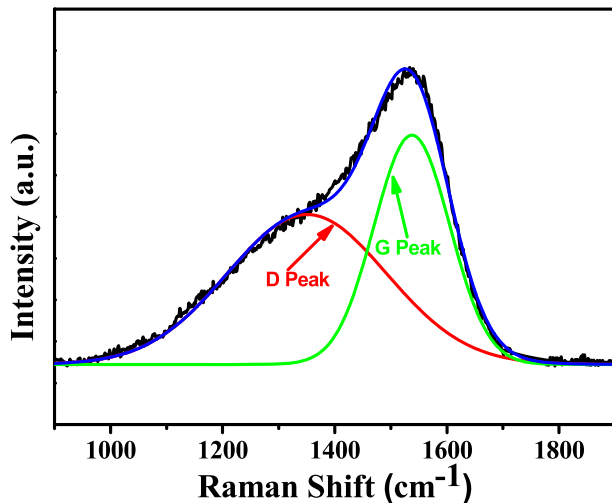


Fig. 4. Representative Raman scattering spectra of Cr/CrC<sub>x</sub>/CrC/DLC.

that the films remain intact during the test and a carbon transferred film formed on the counterpart. The wear tracks are examined by 3D confocal microscopy and the wear rate is shown in Fig. 7(b). A poor wear resistance is observed from the HSS substrate and the wear rate reaches  $(150.3 \pm 0.5) \times 10^{-15} \text{ m}^3/\text{N}\cdot\text{m}$ . On the other hand, the DLC coatings have excellent wear resistance [6,18] as demonstrated by wear rates of  $(1.87 \pm 0.3) \times 10^{-15}$ ,  $(1.59 \pm 0.4) \times 10^{-15}$ ,

$(1.80 \pm 0.3) \times 10^{-15}$ , and  $(1.73 \pm 0.3) \times 10^{-15} \text{ m}^3/\text{N}\cdot\text{m}$  for the 4 samples.

In addition to the mechanical properties and wear resistance, the adhesion between the coating and substrate is a critical factor affecting the service life time. Scratch tests were performed in the progressive mode at a rate of 50 N/min. The acoustic emission signal and scratch pictures are shown in Fig. 8. Fig. 8(a) shows that the critical loads are  $(18 \pm 3) \text{ N}$ ,  $(53 \pm 4) \text{ N}$ ,  $(71 \pm 3) \text{ N}$ , and  $(77 \pm 2) \text{ N}$  for the 4 samples and the scratch morphologies are shown in Fig. 8(b). The best adhesion strength between the Cr/CrC<sub>x</sub>/CrC/DLC coating and HSS substrate is  $L_c = (77 \pm 2) \text{ N}$  and it decreases in the other three samples ( $L_c = (18 \pm 3) \text{ N}$ ,  $(53 \pm 4) \text{ N}$ , and  $(71 \pm 3) \text{ N}$ ) as a result of the distinguishable interface induced by energetic ion bombardment. In order to further demonstrate the significant adhesion enhancement, a thicker DLC coating with a thickness of 50 μm was prepared and the cross-sectional image is depicted in Fig. 9(a). The acoustic emission signal and scratch picture reveal a critical load of  $(73 \pm 3) \text{ N}$  as shown in Fig. 9(b).

#### 4. Discussion

Owing to the high energy ion bombardment at  $-800 \text{ V}$ , the nucleation rate increases and the growth of the columns is disrupted by the nucleation events leading to the reduced average grain size [19]. Therefore, the interlayers exhibit a gradual layered structure beginning with a small-size columnar Cr layer. When the bias is reduced to  $-100 \text{ V}$ , the bombardment effect decreases greatly, and the column structure size increases gradually (Fig. 2).

**Table 2**  
Variations in the D and G peaks for the DLC coatings.

Samples	D band position (cm <sup>-1</sup> )	D FWHMD (cm <sup>-1</sup> )	G band position (cm <sup>-1</sup> )	G FWHMD (cm <sup>-1</sup> )	I <sub>D</sub> /I <sub>G</sub>
Cr/DLC	1341.53	334.66	1532.60	168.12	0.574
Cr/CrC/DLC	1342.08	334.63	1533.16	167.86	0.575
Cr/CrC <sub>x</sub> /DLC	1341.66	333.44	1532.53	168.83	0.573
Cr/CrC <sub>x</sub> /CrC/DLC	1341.24	333.41	1532.27	168.34	0.574

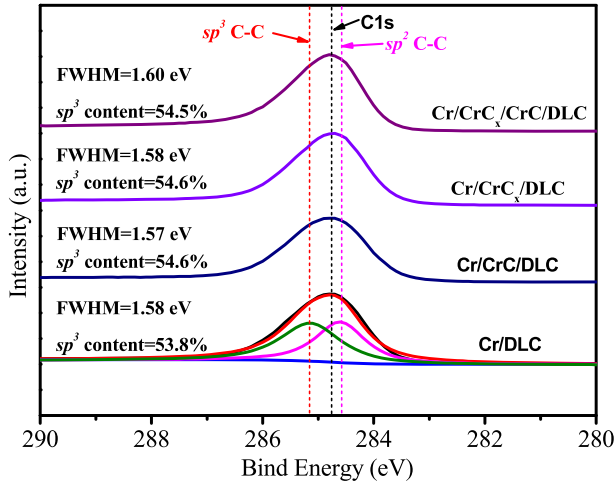


Fig. 5. XPS C1s spectra of the DLC coatings.

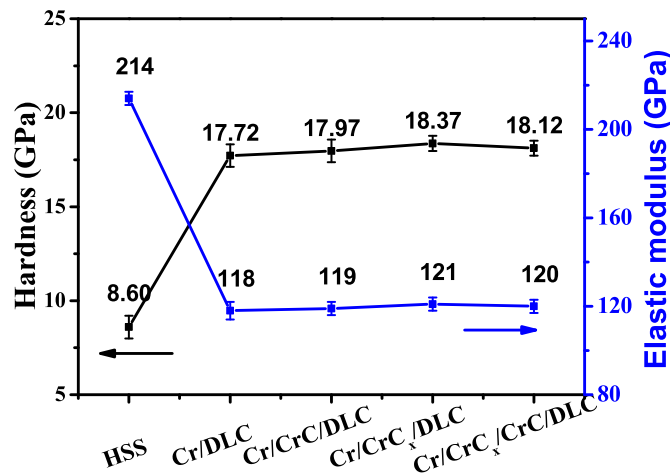


Fig. 6. Hardness and elastic moduli of the HSS and DLC coatings.

**Table 3**  
H<sup>3</sup>/E<sup>2</sup> and H/E ratios of the HSS and DLC coatings.

Samples	H (GPa)	E (GPa)	H <sup>3</sup> /E <sup>2</sup>	H/E
HSS	8.60	214	0.014	0.040
Cr/DLC	17.72	118	0.400	0.150
Cr/CrC/DLC	17.97	119	0.410	0.151
Cr/CrC <sub>x</sub> /DLC	18.37	121	0.423	0.152
Cr/CrC <sub>x</sub> /CrC/DLC	18.12	120	0.413	0.151

With the introduction of C<sub>2</sub>H<sub>2</sub>, an interface is formed (Fig. 2(b)) in the interlayer because the content of C in CrC has a dramatic effect on the morphology and crystal orientation for the reason that Cr–C has a large glass forming ability and wide glass forming range

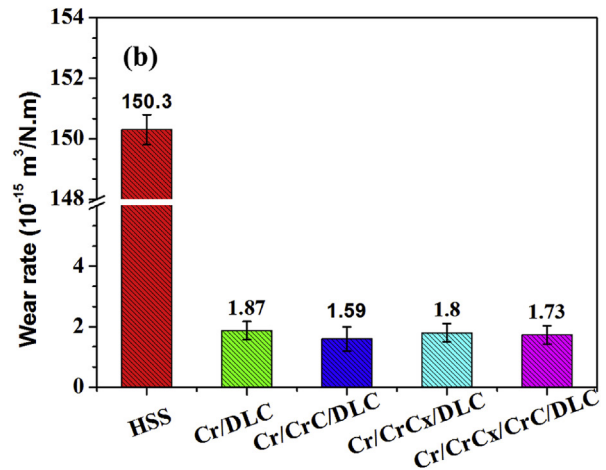
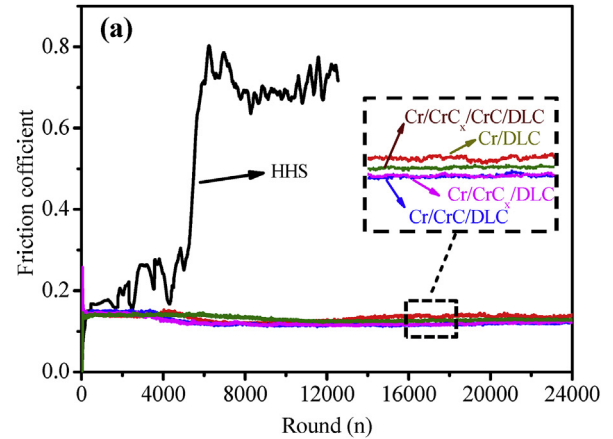


Fig. 7. Friction test of HSS and DLC coatings: (a) Friction coefficients and (b) Wear rates.

compared to other Me–C systems [20,21]. As a result of the significant change of C<sub>2</sub>H<sub>2</sub> in Fig. 2(b), the interface is more obvious than those of other samples. The CrC/DLC interfaces shown in Fig. 2(b) and (d) are indistinct due to superfluous C<sub>2</sub>H<sub>2</sub> in latter CrC deposition and the graded interface produced by carbon implantation [22] compared to the Cr/DLC interface (Fig. 2(a)) and the CrC<sub>x</sub>/DLC interface (Fig. 2(c)) in spite of C ion bombardment.

The DLC coatings show a high hardness (18 ± 0.5 GPa) and a low elastic modulus (120 ± 2 GPa) in the hydrogenated DLC coatings (Fig. 6) due to the content of sp<sup>3</sup> bonding [23–25]. According to the Tunistra-Koenig relationship for amorphous carbon, a small I<sub>D</sub>/I<sub>G</sub> in the Raman spectra usually means a large percentage of sp<sup>3</sup> bonding and high hardness [26–28]. The I<sub>D</sub>/I<sub>G</sub> ratio of our sample is 0.57 ± 0.01 on account of the relatively high hardness of the hydrogenated DLC coatings (Fig. 4). XPS (Fig. 5) also shows that the sp<sup>3</sup> content reaches 54.5% arising from the proper bias and low

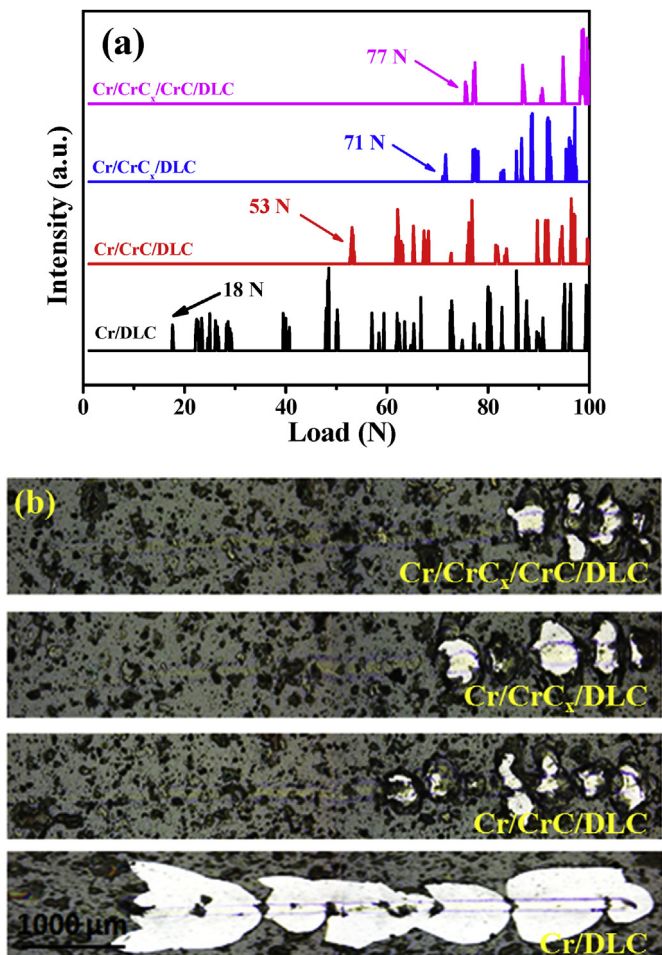


Fig. 8. Scratch test results of the DLC coatings: (a) Acoustic emission signal and (b) Scratch morphology.

substrate temperature ( $<200\text{ }^{\circ}\text{C}$ ). It has been shown that the largest  $\text{sp}^3$  fractions are formed by  $\text{C}^+$  bombardment at  $100\text{ eV}$  [29,30]. If the energy is small, ions just stick to the surface and have the lower energy state that forms  $\text{sp}^2$  [31]. However, if the energy is too high, heat is generated [32]. Here, the negative pulsed high voltage ( $7.5\text{ kV}$ ,  $50\text{ Hz}$ ,  $100\text{ }\mu\text{s}$ ) is used to increase the ion energy and a small pulse duration (0.5%) is used to limit the temperature rise. Therefore, ion bombardment removes the  $\text{sp}^2\text{-C}$  atoms sticking onto the surface and increases the  $\text{sp}^3$  content and coating density. At the same time, the low substrate temperature ( $<200\text{ }^{\circ}\text{C}$ ) prevents transformation to graphite which occurs at  $300\text{--}500\text{ }^{\circ}\text{C}$ . The cold cathode structure of the anode layer ion source reduces the temperature increase. It is noted that a relatively small elastic modulus ( $120 \pm 2\text{ GPa}$ ) is observed from the DLC coatings. As described by Lawn and Pharr, larger  $\text{H}^3/\text{E}^2$  and  $\text{H}/\text{E}$  ratios indicate better toughness and wear resistance [33–35]. With a large  $\text{H}/\text{E}$  ratio, the film surface can respond to external force by elastic recovery rather than plastic deformation to reduce wear [36]. The  $\text{H}^3/\text{E}^2$  ( $0.41 \pm 0.1$ ) and  $\text{H}/\text{E}$  ( $0.151 \pm 0.001$ ) ratios of our samples are larger than those presented in our previous work [37–40], indicating high wear resistance of these DLC coatings. The high  $\text{H}/\text{E}$  ( $\text{H}^3/\text{E}^2$ ) and low friction coefficient (0.12) arising from the self-lubricating effects produce a low wear rate of  $(1.7 \pm 0.2) \times 10^{-15}\text{ m}^3/\text{N}\cdot\text{m}$  (Fig. 7).

There is noticeable improvement in adhesion between the DLC coating and substrate ( $(77 \pm 2)\text{ N}$ ) compared to the other three samples ( $L_c = (18 \pm 3)\text{ N}$ ,  $(53 \pm 4)\text{ N}$ ,  $(71 \pm 3)\text{ N}$ ) as shown in Fig. 8.

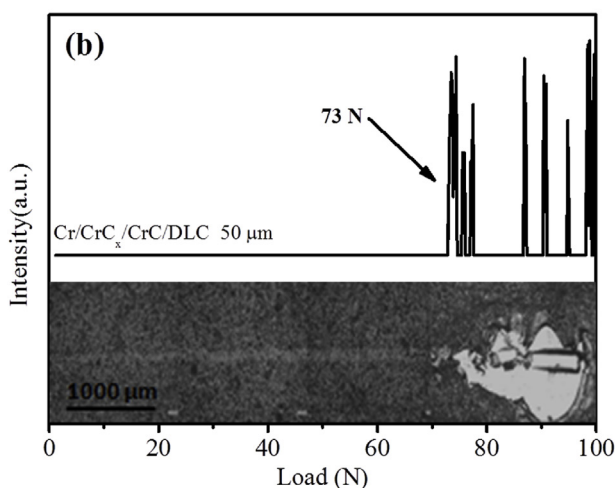
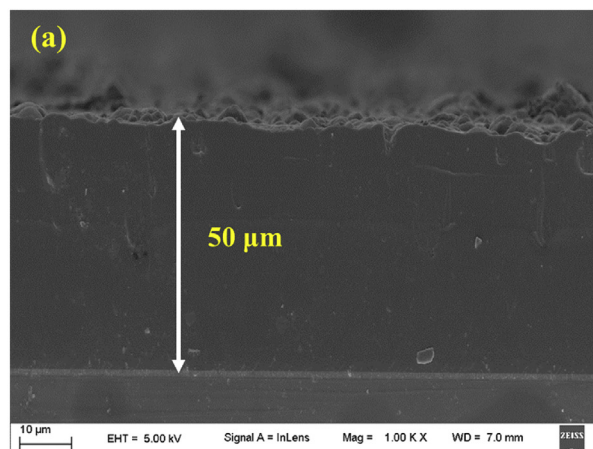
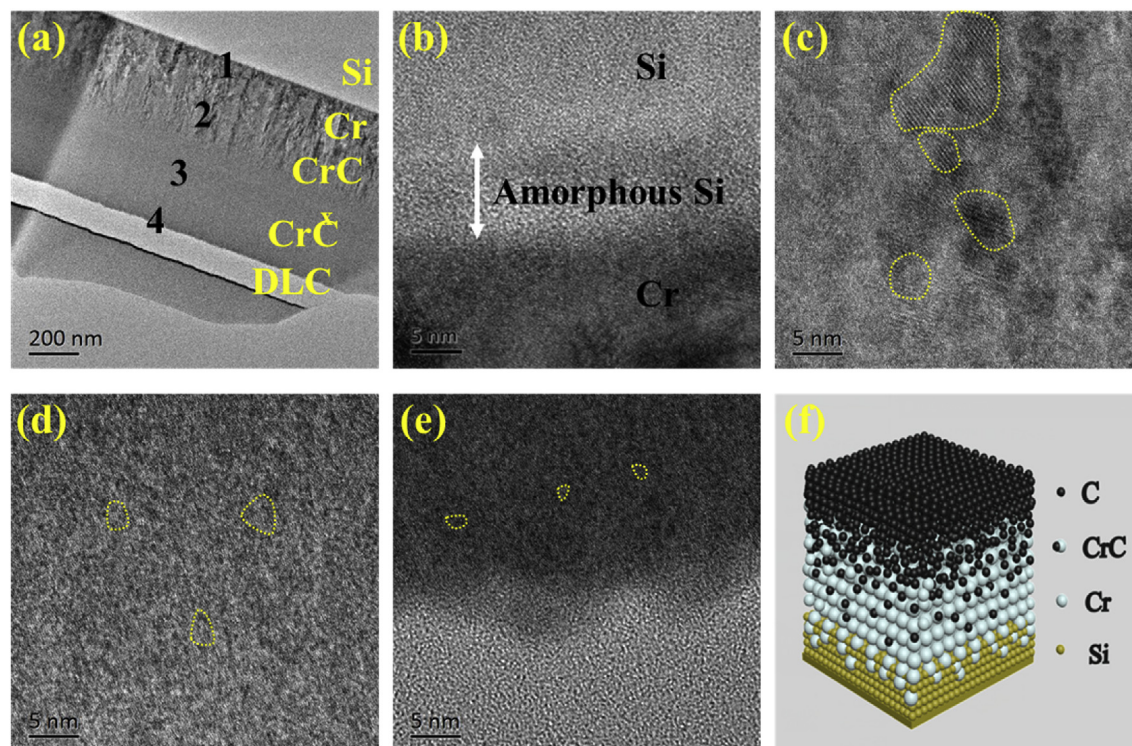


Fig. 9. (a) SEM cross-sectional images and (b) Scratch test of the  $50\text{ }\mu\text{m}$  DLC coating.

Even when thickness is increased to  $50\text{ }\mu\text{m}$ , excellent adhesion is still observed ( $L_c = (73 \pm 3)\text{ N}$ ). In order to explain the excellent adhesion, the cross-sectional TEM image of the  $\text{Cr}/\text{CrC}_x/\text{CrC}/\text{DLC}$  sample is shown in Fig. 10(a) and the interfaces between different layers are presented in Fig. 10(b–e) corresponding to labels 1, 2, 3, and 4 in Fig. 10(a). No obvious defects such as macro-particles, voids, etc. can be observed from the substrate to the DLC coating, even at the interfaces between layers with different composition. Owing to energetic Cr ion bombardment [41,42], a  $5\text{ nm}$  amorphous Si layer is formed on the surface of the Si substrate as shown in Fig. 10(b). With ion bombardment, Cr starts to grow and crystallize gradually on the amorphous layer thereby avoiding the lattice mismatch between the Si substrate and Cr interlayer and producing high adhesion [43,44]. Simultaneous interface diffusion and compounding take place between the Si substrate and Cr interlayer because of the high ion energy [41,45] to improve adhesion further. With the introduction of  $\text{C}_2\text{H}_2$ , the crystallinity of Cr is restrained [19,46] and a composite structure composed of nanocrystalline  $\text{CrC}_x$  particles homogeneously embedded in the amorphous  $\text{CrC}_x$  base is formed as shown in Fig. 10(c). The CrC layer is prepared in a superfluous  $\text{C}_2\text{H}_2$  atmosphere and the size of the nanocrystals is further restricted to about  $2\text{--}4\text{ nm}$  as shown in Fig. 10(d). The evolution from crystallized Cr to nanocrystalline/amorphous CrC is continuous and gradual and no obvious interface is formed because of the gradually increasing  $\text{C}_2\text{H}_2$  flow (Table 1). Fig. 10(e) depicts the



**Fig. 10.** (a) Cross-sectional image of Cr/CrCx/CrC/DLC; (b–e) High-magnification images of positions 1, 2, 3, and 4; (f) Sketch map of Si/Cr/CrCx/CrC/DLC.

interface between the CrC interlayer and DLC coating, showing a continuous microstructure from the nanocrystalline/amorphous CrC layer to the amorphous DLC coating suggesting no lattice mismatch. At the same time, on account of C ion bombardment and implantation, the CrC interlayer with abundant carbon can form strong covalent bonds with the DLC coatings [13,47,48] and no macro-particles or large-scale defects can be found from the interface. A 3D schematic shows the component transition from the substrate (Si) to the interlayer (Cr/CrCx/CrC), and DLC coating is presented in Fig. 10(e). Both the brittle hetero-interfaces (one between the substrate and Cr interlayer and the other between the CrC interlayer and DLC coating) are connected by diffusion and compounding of atoms on both sides. This results in small differences in the physical properties such as the thermal expansion coefficient between the substrate, interlayer and coating. The excellent adhesion results from the continuous transition from the substrate to the interface and coating and strong covalent bond produced by energetic Cr ion bombardment and C ion implantation.

## 5. Conclusion

In order to improve the adhesion strength of thick DLC films, an ion-assisted interfacial treatment together with introduction of a gradient interlayer is implemented. To obtain highly ionized and energetic Cr and C ions, HiPIMS and an anode layer ion source are coupled at a large bias in PIII&D. A large hardness of 18.4 GPa, small friction coefficient of 0.12, and small wear rate of  $(1.7 \pm 0.2) \times 10^{-15} \text{ m}^3/\text{N} \cdot \text{m}$  are observed. Because of the defect-free transition from the HSS substrate to the interlayer and then the DLC coating, excellent adhesion with the critical load of 77 N is achieved when the thickness of DLC coating is more than 10  $\mu\text{m}$ . Even for a DLC film with a thickness of 50  $\mu\text{m}$ , 73 N is observed. The relationship between the interface and the coating structure, morphology, and mechanical properties is discussed. This

interlayer design strategy may be used for future manufacturing of thick DLC films.

## Acknowledgements

This work was financially supported by National Materials Genome Project (No. 2016YFB0700600), Shenzhen Science and Technology Research Grants (JCYJ20150828093127698), and City University of Hong Kong Applied Research Grant (ARG) No. 9667122.

## References

- [1] J. Robertson, Diamond-like amorphous carbon, *Mater. Sci. Eng. R* 37 (2002) 129–281.
- [2] M. Pandey, D. Bhattacharyya, D.S. Patil, K. Ramachandran, N. Venkatramani, A.K. Dua, Structural and optical properties of diamond like carbon films, *J. Alloys Compd.* 386 (2005) 296–302.
- [3] T.S. Santra, C.H. Liu, T.K. Bhattacharyya, P. Patel, T.K. Barik, Characterization of diamond-like nanocomposite thin films grown by plasma enhanced chemical vapor deposition, *J. Appl. Phys.* 107 (2010) 124320.
- [4] Y. Chen, J.M. Wu, X.Y. Nie, S.F. Yu, Study on failure mechanisms of DLC coated Ti6Al4V and CoCr under cyclic high combined contact stress, *J. Alloys Compd.* 688 (2016) 964–973.
- [5] A.H. Lettington, Applications of diamond-like carbon thin films, *Philos. Trans. Royal Soc. B Biol. Sci.* 342 (1998) 555–560.
- [6] A. Grill, Diamond-like carbon: state of the art, *Diam. Relat. Mater.* 8 (1999) 428–434.
- [7] X. Wang, W. Wu, S. Li, et al., Properties of W incorporated diamond-like carbon films prepared by pulsed-laser deposition, *J. Alloys Compd.* 479.1 (2009) 741–745.
- [8] D. Wei, A. Wang, Deposition and properties of Al-containing diamond-like carbon films by a hybrid ion beam sources, *J. Alloys Compd.* 509 (2011) 4626–4631.
- [9] M. Lubwama, B. Corcoran, K. Sayers, J.B. Kirabira, A. Sebbit, K.A. McDonnell, D. Dowling, Adhesion and composite micro-hardness of DLC and Si-DLC films deposited on nitrile rubber, *Surf. Coating. Technol.* 206 (2012) 4881–4886.
- [10] A.Y. Wang, H.S. Ahn, K.R. Lee, J.P. Ahn, Unusual stress behavior in W-incorporated hydrogenated amorphous carbon films, *Appl. Phys. Lett.* 86 (2005) 111902.
- [11] M. Kalin, I. Velkavrh, J. Vizintin, L. Ozbolt, Review of boundary lubrication

- mechanisms of DLC coatings used in mechanical applications, *Meccanica* 43 (2008) 623–637.
- [12] A. Anttila, R. Lappalainen, V.M. Tiainen, M. Hakovirta, Superior attachment of high-quality hydrogen-free amorphous diamond films to solid materials, *Adv. Mater.* 9 (1997) 1161–1164.
- [13] B.H. Lung, M.J. Chiang, M.H. Hon, Effect of gradient a-SiC<sub>x</sub> interlayer on adhesion of DLC films, *Mater. Chem. Phys.* 72 (2001) 163–166.
- [14] Z. Wu, X. Tian, Y. Wei, C. Gong, S. Yang, F. Pan, P.K. Chu, Graded nano-structured interfacial layers fabricated by high power pulsed magnetron sputtering - plasma immersion ion implantation and deposition (HPPMS-PIII&D), *Surf. Coating. Technol.* 236 (2013) 320–325.
- [15] M. Tabbal, M. Chaker, M.A.E. Khakani, E.G. Herbert, B.N. Lucas, Effect of laser intensity on the microstructural and mechanical properties of pulsed laser deposited diamond-like-carbon thin films, *J. Appl. Phys.* 85 (1999) 3860–3865.
- [16] E. Enríquez, M.A.D.L. Rubia, A.D. Campo, et al., Characterization of carbon nanoparticles in thin-film nanocomposites by confocal Raman microscopy, *J. Phys. Colloid Chem.* 1181 (19) (2014) 10488–10494.
- [17] E. Ech-Chamikh, A. Essaifi, Y. Ijdiyaou, M. Azizan, XPS study of amorphous carbon nitride (a-C: N) thin films deposited by reactive RF sputtering, *Sol. Energy Mater. Sol. Cell.* 90 (2006) 1420–1423.
- [18] Y. Sun, Z. Chai, X. Lu, et al., Tribological performance of a tungsten disulfide lubricant film prepared by atomic layer deposition using tungsten hexacarbonyl and hydrogen sulfide as precursors, *Tribol. Int.* 114 (2017) 478–484.
- [19] I. Petrov, P.B. Barna, L. Hultman, J.E. Greene, Microstructural evolution during film growth, *J. Vacuum Sci. Technol. A Vacuum Surf. Films* 21 (2009) S117–S128.
- [20] K. Nygren, M. Andersson, J. Högström, W. Fredriksson, K. Edström, L. Nyholm, U. Jansson, Influence of deposition temperature and amorphous carbon on microstructure and oxidation resistance of magnetron sputtered nanocomposite CrC films, *Appl. Surf. Sci.* 305 (2014) 143–153.
- [21] U. Jansson, E. Lewin, Sputter deposition of transition-metal carbide films - a critical review from a chemical perspective, *Thin Solid Films* 536 (2013) 1–24.
- [22] K.C. Walter, M. Nastasi, C. Munson, Adherent diamond-like carbon coatings on metals via plasma source ion implantation, *Surf. Coating. Technol.* 93 (1997) 287–291.
- [23] P. Yang, J.Y. Chen, Y.X. Leng, H. Sun, N. Huang, P.K. Chu, Effect of annealing on structure and biomedical properties of amorphous hydrogenated carbon films, *Surf. Coating. Technol.* 186 (2004) 125–130.
- [24] J.X. Guo, Z. Sun, B.K. Tay, X.W. Sun, Field emission from modified nanocomposite carbon films prepared by filtered cathodic vacuum arc at high negative pulsed bias, *Appl. Surf. Sci.* 214 (2003) 351–358.
- [25] W. Gou, G. Li, X. Chu, B. Zhong, Effect of negative self-bias voltage on microstructure and properties of DLC films deposited by RF glow discharge, *Surf. Coating. Technol.* 201 (2007) 5043–5045.
- [26] M. Jelínek, K. Smetana, T. Kocourek, B. Dvořánková, J. Zemek, J. Remsa, T. Luxbacher, Biocompatibility and sp<sup>3</sup>/sp<sup>2</sup> ratio of laser created DLC films, *Mater. Sci. Eng. B* 169 (2010) 89–93.
- [27] A.C. Ferrari, J. Robertson, Resonant Raman spectroscopy of disordered, amorphous, and diamondlike carbon, *Phys. Rev. B Condensed Matter* 64 (2001) 075414.
- [28] F. Tuinstra, J.L. Koenig, Raman spectrum of graphite, *J. Chem. Phys.* 53 (1970) 1126–1130.
- [29] D.R. McKenzie, Tetrahedral bonding in amorphous carbon, *Rep. Prog. Phys.* 59 (1999) 1611–1664.
- [30] Y. Lifshitz, Diamond-like carbon -present status, *Diam. Relat. Mater.* 8 (1999) 1659–1676.
- [31] J. Robertson, The deposition mechanism of diamond-like a-C and a-C: H, *Diam. Relat. Mater.* 3 (1994) 361–368.
- [32] H. Hofsäss, H. Feldermann, R. Merk, M. Sebastian, C. Ronning, Cylindrical spike model for the formation of diamondlike thin films by ion deposition, *Appl. Phys. A* 66 (1998) 153–181.
- [33] A. Leyland, A. Matthews, On the significance of the H/E ratio in wear control: a nanocomposite coating approach to optimised tribological behaviour, *Wear* 246 (2000) 1–11.
- [34] B.R. Lawn, A.G. Evans, D.B. Marshall, Elastic/plastic indentation damage in ceramics: the median/radial crack system, *J. Am. Ceram. Soc.* 63 (1980) 574–581.
- [35] J. Halling, The tribology of surface films ☆, *Thin Solid Films* 108 (1983) 103–115.
- [36] C.A. Charitidis, Nanomechanical and nanotribological properties of carbon-based thin films: a review, *Int. J. Refract. Metals Hard Mater.* 28 (2010) 51–70.
- [37] Y.T. Pei, D. Galvan, J.T.M. De Hosson, A. Cavaleiro, Nanostructured TiC/a-C coatings for low friction and wear resistant applications, *Surf. Coating. Technol.* 198 (2005) 44–50.
- [38] A.Y. Wang, K.R. Lee, J.P. Ahn, J.H. Han, Structure and mechanical properties of W incorporated diamond-like carbon films prepared by a hybrid ion beam deposition technique, *Carbon* 44 (2006) 1826–1832.
- [39] A. Voevodin, Design of a Ti/TiC/DLC functionally gradient coating based on studies of structural transitions in Ti–C thin films, *Thin Solid Films* 298 (1997) 107–115.
- [40] N. Savvides, T.J. Bell, Microhardness and Young's modulus of diamond and diamondlike carbon films, *J. Appl. Phys.* 72 (1992) 2791–2796.
- [41] B.Y. Tsaor, Z.L. Liao, J.W. Mayer, Ion-beam-induced silicide formation, *Appl. Phys. Lett.* 34 (1979) 168–170.
- [42] Z.L. Liao, B.Y. Tsaor, J.W. Mauer, Influence of atomic mixing and preferential sputtering on depth profiles and interfaces, *J. Vac. Sci. Technol.* 16 (1979) 121–127.
- [43] Z. Yang, J. Lian, J. Wang, Molecular dynamics simulation of thin film interfacial strength dependency on lattice mismatch, *Thin Solid Films* 537 (2013) 190–197.
- [44] P. Gröning, S. Nowak, L. Schlappbach, Surface modifications of nitrogen-plasma-treated stainless steels, *Appl. Surf. Sci.* 64 (1993) 265–273.
- [45] A. Hiraki, E. Lugujo, M.A. Nicolet, J.W. Mayer, Low-temperature migration of silicon through metal films importance of silicon-metal interface, *Phys. Status Solidi* 7 (1971) 401–406.
- [46] K. Nygren, M. Samuelsson, A. Flink, H. Ljungcrantz, Å.K. Rudolphi, U. Jansson, Growth and characterization of chromium carbide films deposited by high rate reactive magnetron sputtering for electrical contact applications, *Surf. Coating. Technol.* 260 (2014) 326–334.
- [47] E.R. Petry, C.D. Boeira, F. Cemin, L.M. Leidens, L.T. Bim, D.G. Larrude, M.E.H.M.D. Costa, C.A. Figueroa, Physicochemical structure of SiC<sub>x</sub>:H to improve DLC adhesion on steel, *Surf. Eng.* 32 (2016) 1–7.
- [48] F. Cemin, L.T. Bim, L.M. Leidens, M. Morales, I.J. Baumvol, F. Alvarez, C.A. Figueroa, Identification of the chemical bonding prompting adhesion of a-C: H thin films on ferrous alloy intermediated by a SiC<sub>x</sub>:H buffer layer, *ACS Appl. Mater. Interfaces* 7 (2015) 15909–15917.